Chapter 4

Harmonic Distortion Caused by Single-Phase Grid-Connected PV Inverter

Yang Du and Dylan Dah-Chuan Lu

Additional information is available at the end of the chapter

http://dx.doi.org/10.5772/intechopen.73030

Abstract

Due to the fast growth of photovoltaic (PV) installations, concerns are rising about the harmonic distortion generated from PV inverters. A general model modified from the conventional control structure diagram is introduced to analyze the harmonic generation process. Causes of the current harmonics are summarized, and its relationship with output power levels is analyzed. In particular for two-stage inverter, unlike existing models that assume the direct current (DC)-link voltage is constant, the DC-link voltage ripple is identified as the source of a series of odd harmonics. The inverter is modeled as a time-varying system by considering the DC-link voltage ripple. A closed-form solution is derived to calculate the amplitude of the ripple-caused harmonics. The theoretical derivation and analysis are verified by both simulation and experimental evaluation.

Keywords: DC-link voltage ripple, harmonics, Matlab/Simulink, PV inverter, single phase

1. Introduction

Among numerous renewable energy sources, solar energy is considered as one of the most promising resources for large-scale electricity production [1]. In several countries including Australia, an increasing number of photovoltaic (PV) generation systems are connected to the distribution network as a result of strong government support. The PV market is growing rapidly (30–40%), and its price is constantly decreasing. Many countries are trying to increase the penetration of renewable energy.

The power electronics interface is essential for connecting renewable energy sources to the grid. This interface has two main functions such as extracting the maximum amount of power from the PV modules [2, 3] and conversion of direct current (DC) power to an appropriate

form of alternative current (AC) power for the grid connection. Renewable energy sources such as solar energy cannot be manipulated in the same way as conventional power sources, so the operating conditions of PV inverters vary according to the solar insolation [4]. However, utility standards and manufacturers' data sheets are only concerned with the full-load condition.

PV systems incorporate power electronic interfaces, which generate a level of harmonics [5], potentially causing current and voltage distortions. The summations of various higher frequency sinusoidal components are the harmonics of current or voltage waveforms, which are an integer multiple of the fundamental frequency. These harmonics have a great influence on the operational efficiency and reliability of the power system, loads, and protective relaying [6]. Due to the rapid growth of PV installations, attention to harmonic distortion introduced by PV inverters to the grid is on the rise.

The degree of current total harmonic distortion (THD), as a ratio of the fundamental current and the real power output of the inverter, vary significantly [7]. At a low power output level, the current THD becomes higher, especially for generated power below 20% of the rated power, such as in the morning or evening. Many researchers have reported this phenomenon and tried to find out the causes. In the control system, the quantization and resolution effects of the measurement devices have been pointed out as one of the causes [8]. Another explanation is that the closed-loop current controls, which are intended to minimize the harmonic components, stop working at a low power output level [7]. Some researchers have suggested that the DC-link voltage regulation is highly related to the reference current resolution [9]. However, the comprehensive and systematic analysis of the generation process of the harmonics in the PV inverter output current is missing.

The conventional model of current control structure [10] is widely used to design the control loop and to analyze its stability. However, this model dose not including harmonic information, and the model cannot reflect the influence of the control schemes on the resulted harmonics. Section 2 introduces a general model modified from a conventional control structure diagram to analyze the harmonic generation process. The "harmonic impedance" concept [10] is used to quantitatively calculate the harmonic amplitude caused by each source. This is important because of the growing concern of harmonics generated by these devices and their effect upon other equipment.

A series of fund odd harmonics cannot be completely explained by the factors usually examined in such cases. These harmonics are caused by the DC-link voltage ripple, and a time-varying model is proposed to analyze this phenomenon in Section 4.

In order to analyze and design the PV inverter, the DC-link voltage is assumed as constant in the traditional model of a PV inverter. However, this is not always the case. The AC instantaneous output power exhibits a pulsation at the double-line frequency for single-phase grid-connected inverters. Under stable insolation conditions, the DC output voltage of the PV modules is controlled as constant at the maximum power point (MPP). Therefore, the power pulsation caused by single-phase power generation is converted into the static stored energy on the decoupling capacitor, and the double-line frequency of voltage ripple can be found at the DC link [11–13]. By using large electrolytic capacitors, the ripple can be reduced but not

eliminated. However, the electrolytic parts have far more limited life than the applications [14] which need to be avoided.

A single-stage inverter is shown in **Figure 1(a)**; an efficient maximum power point tracking (MPPT) process is realized by a large power decoupling capacitor. Hence, modeling the inverter can use adaptable constant DC-link voltage assumption in this linear model. However, as two-stage inverter is shown in **Figure 1(b)**, the power decoupling capacitor is placed at the high-voltage DC link. In this topology, a larger voltage ripple is allowed to present across a DC link in order to minimize the decoupling capacitor [15], hence the constant DC-link voltage assumption is not valid.

The three-phase bridge converter for harmonic transfer is investigated in [16], the voltage second harmonic on a DC link producing a third harmonic on the AC side can be found. However, the DC-link voltage also causes output current frequency spectrum for the fifth, seventh, and a series of odd harmonics [17]. The explanation of this phenomenon cannot be found in the previous research. Many methods have been proposed to eliminate the current harmonics caused by the DC-link ripple without analyzing the harmonics generation process. A specifically designed pulse-width modulation (PWM) control algorithm [18] is proposed to compensate the DC-link voltage ripple. In [19], a control technique, which allows for 25% ripple voltage without distorting the output current waveform, has been proposed. The cutoff frequency of this design is 10 Hz, which could attenuate the voltage ripple in the control loop, but dynamic performance is decreased in this system. The main purpose of all these works is to eliminate the effects of the DC-link voltage ripple. However, an understanding of the relationship and the analytical model for qualitative information between the output current harmonics and DC-link voltage ripple is still missing.

In this chapter, for harmonic analysis studies, a new model of the single-phase full-bridge PV inverter is proposed by regarding its loading level and the ripple of the DC-side voltage. It is obtained by adding representation of the DC-link voltage ripple into the conventional linear model of a grid-connected PV inverter. Thus, it becomes a periodical time-varying model.

This chapter is organized as follows: a general model with harmonic information is introduced in Section 2. In Section 3, the double-line frequency voltage ripple on the DC link is identified as the cause of a series of odd harmonics. A time-varying model is proposed to analyze this phenomenon. Section 4 gives simulation and experimental results, which verify the validity of the proposed model and solution. Conclusions are given in Section 5.

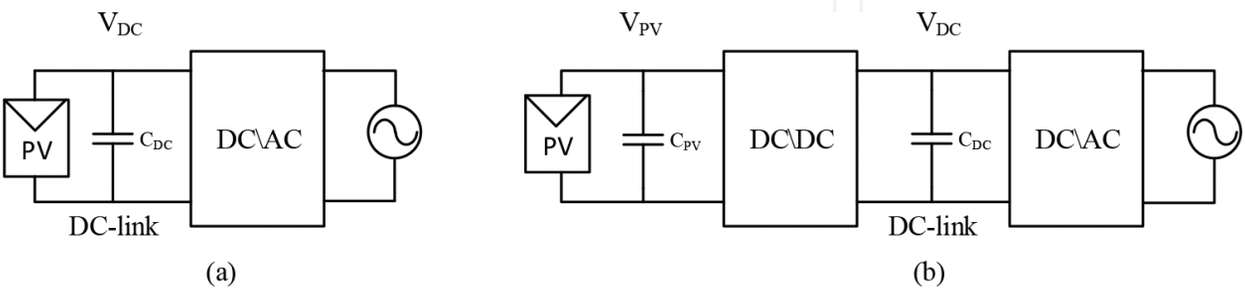

Figure 1. Block diagram of (a) single-stage inverter and (b) two-stage inverter.

2. Modeling of the PV inverter for harmonic analysis

In this section, PWM inverter framework with current feedback control for single-phase full-bridge PV inverter, which is generally used in the commercial products, conventional model of the current regulation scheme for that kind of inverter, and general inverter model proposed for the harmonic analysis are presented.

2.1. Single-phase full-bridge PV inverter with current control

An example of PWM inverter framework with current feedback control is shown in **Figure 2**. It is the most common structure which used by the commercial products. The inverter is formed by one output inductor, a DC-link capacitor C_{DC}, and four power switches. The DC-link voltage V_{DC} presents two different scenarios: one is with voltage ripple and another is without voltage ripple. The following sections analyze these two different cases separately. V_{inv} is the full-bridge inverter output voltage and V_g is the grid voltage, I_{out} is the inverter output current. A fixed grid voltage has been applied to the grid-connected inverter output terminals, and the inverter input voltage is controlled to provide MPP tracking. A current control scheme is used, since only the AC output current can be controlled. A filter has been used to connect between the inverter and the grid. In this chapter, a single inductor is used to simplify the analysis. A feedback control with the PI controller is used for the PWM inverter

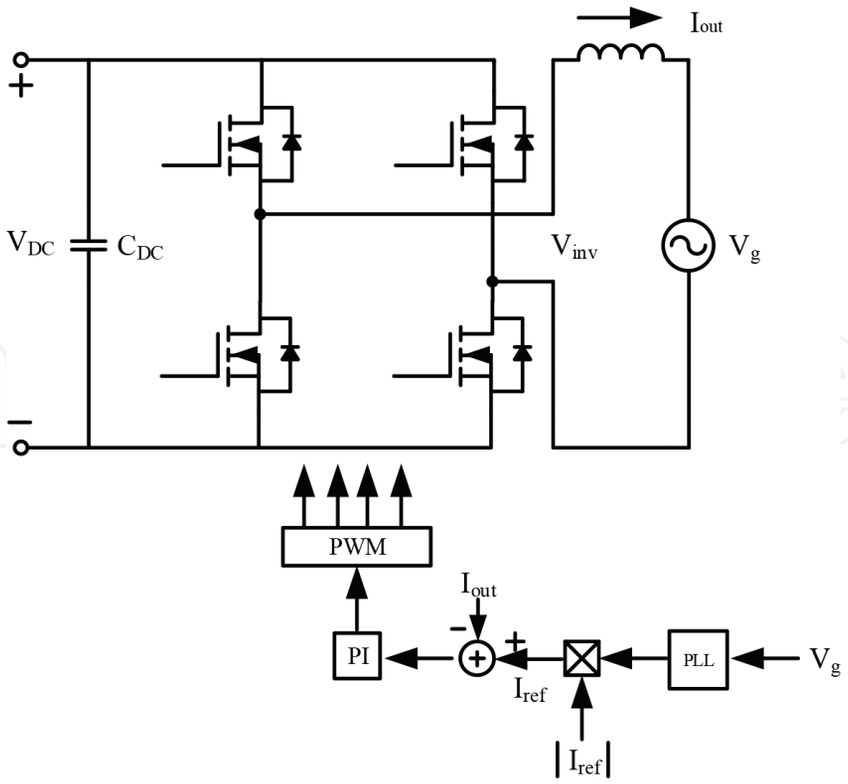

Figure 2. PWM inverter framework with current-controlled feedback loop.

to control the output current I_{out} to track a reference output current I_{ref}. A phase-locked loop (PLL) has been used to obtain the phase angle of I_{ref} from the grid voltage V_g. The amplitude of the reference current $|I_{ref}|$ can be determined by the voltage control loop according to the MPPT process. The design of the voltage control loop may vary according to different inverter topologies. The detailed derivation of $|I_{ref}|$ can be found in [10, 20].

2.2. Conventional model of current regulation scheme

Figure 3 shows the conventional control structure diagram of the current-controlled inverter. This model can be analyzed by using conventional linear analysis methods. It can help the designer to tune the controller [21] and investigate the control performance and stability [22]. The closed-loop transfer function is given by

$$I_{out} = \frac{G_{PI}G_{PWM}G_{inv}G_f}{1 + G_{PI}G_{PWM}G_{inv}G_f} I_{ref} - \frac{G_f}{1 + G_{PI}G_{PWM}G_{inv}G_f} V_g \tag{1}$$

where G_{PI}, G_{PWM}, G_{inv}, and G_f are the transfer functions for the PI controller, PWM, inverter, and filter, respectively. In this model, only the fundamental waveforms are considered, and harmonic information is required for the harmonic distortion analysis.

2.3. The general inverter model for the harmonic analysis

Figure 4 shows the generalized model which is derived from the conventional current control structure diagram for a PWM inverter with harmonic information. The location and types of harmonic sources, which need to be added, are shown in this figure. The output current *S5* is generated based on a reference current by the full-bridge inverter with current control, as shown in the first trace. The model of current control scheme, which includes the harmonics information, is shown in the second trace. Compared with **Figure 3**, the switch harmonic source $V_{switch\ harmonics}$ in the PWM section is added to generate a pulse waveform on top of the sinusoidal signal. This harmonic source contains the characteristic of the PWM, including the type of PWM method and the switching frequency. The voltage difference between the grid voltage and the inverter output voltage will cause the changes in the output current. Therefore, in **Figure 4**, the grid voltage harmonic source is added at the inverter

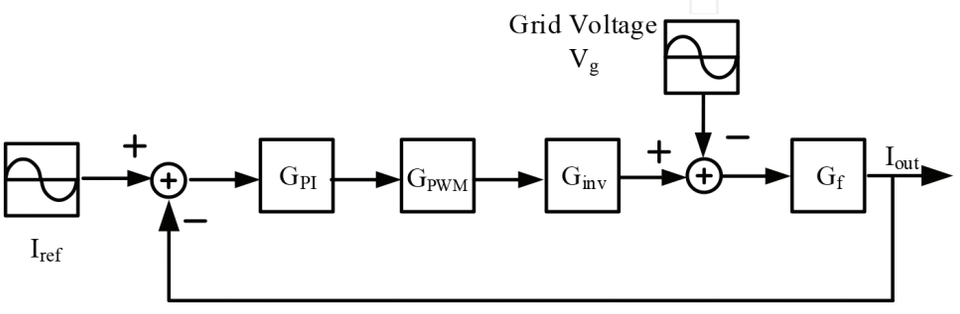

Figure 3. Conventional control structure diagram of the current-controlled inverter.

section. The lowest trace in **Figure 4** sketches the waveform of each stage, and the details are described as follows:

1. *S1* is the error between the current reference and the output current of the inverter, $S1 = I_{ref} - I_{out} = I_{ref} - S5$.
2. *S*2 is the amplitude modulation (AM) ratio, $S2 = S1G_{PI}$, where the PI controller's transfer function is $G_{PI} = k_p + k_i/s$. k_p and k_i are the proportional and the integral gain.
3. *S*3 is the gate drive signal. $S3 = S2G_{PWM} + V_{switch\ harmonics}$, where $G_{PWM} = 1/C_{pk}$ and C_{pk} is the carrier signal's peak value.
4. *S*4 is the output voltage of the inverter V_{inv}, $S4 = S3G_{inv}$, where $G_{inv} = V_{DC}$. The V_{DC} can be either a time-varying or a constant signal; these two cases need to be treated separately.
5. *S*5 is the output current of the inverter I_{out}. $S5 = (S4 - V_g)G_f$. The grid voltage V_g may contain the voltage harmonics $V_{g\ harmonics}$.$S4 - V_g$ is the voltage difference between the output filter. The transfer function of the filter is $G_f = 1/(Ls)$, where L is the filter's inductance.

The main causes of harmonic in PV inverter can be summarized into several categories: grid background voltage distortion, switch harmonics (high frequency), DC-link voltage variation due to MPPT, and some other causes (PLL blocks, etc.). Harmonic distortion for both cases, with or without voltage ripple on the DC link, can be analyzed by using this generalized model.

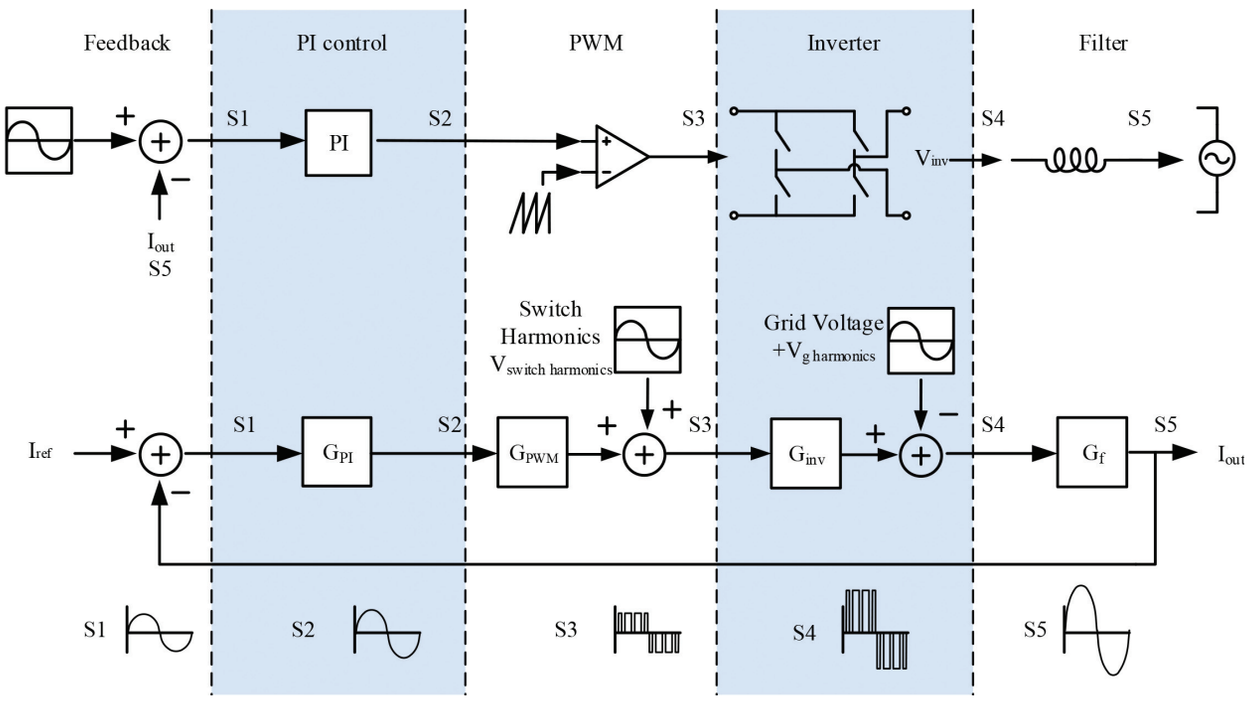

Figure 4. Model of current-controlled PWM inverter with harmonic information.

3. Current harmonic caused by DC-link voltage ripple

In this section, the current harmonics caused by DC-link voltage ripple has been analyzed. The model for considering the double-line frequency voltage ripple has been built. The closed-form solution for the current harmonics has been provided.

Figure 5 shows the model of the inverter based on **Figure 4**, and the DC-link voltage ripple has been taken into account. The inverter transfer function G_{inv} shown in **Figure 4** is replaced by the section under the triangle shading, which is a sinusoidal signal V_{rip} at double-line frequency on top of the DC component V_{DC}. Since the voltage ripple is time-varying, the transfer function for this section cannot be derived. In [23], the authors point out that closed-form solutions cannot be derived when the harmonic ripple components are not neglected. However, numeric solutions can be evaluated for any particular operating condition by using this model.

The harmonic characteristics of the output current shown in **Figure 5** can be identified by qualitatively analyzing the simplified loop model. The section under the triangle shading is also known as the amplitude modulation; the feedback loop with unit delay is shown in **Figure 6**, where Z^{-1} denotes the delay of a unit sample period. Compared with **Figure 6**, in this simplified model, several linear blocks are left out. Due to the system linearity, the signal frequency characteristics will remain the same. A similar analysis method, which has been used in sound processing research [24], is adopted in this chapter to analyze this time-varying system. Two discrete-time sinusoidal example signals $I_{ref}[n] = \cos(\omega_o n)$ *and* $V_{rip}[n] = \cos(2\omega_o n)$ are used. The output signal $y[n]$ can be illustrated as the result of subtraction between the reference signal $\cos(\omega_o n)$ and the delayed output signal $y[n-1]$ then timed with the AM section, which is $\cos(2\omega_o n) + V_{DC}$

$$\begin{aligned} y[n] &= [\cos(\omega_o n) - y[n-1]][\cos(2\omega_o n) + V_{DC}] \\ &= \cos(\omega_o n)[\cos(2\omega_o n) + V_{DC}] - y[n-1][\cos(2\omega_o n) + V_{DC}] \end{aligned} \tag{2}$$

For $n \leq 0$, ω_o is the angular velocity of a signal in the fundamental frequency, $V_{DC}$is constant, at the initial condition, $y[n] = 0$,. The delay exists at any point in time n, and we need to store $y[n-1]$ so that it can be used in the computation of $y[n]$. The $y[n-1]$ is

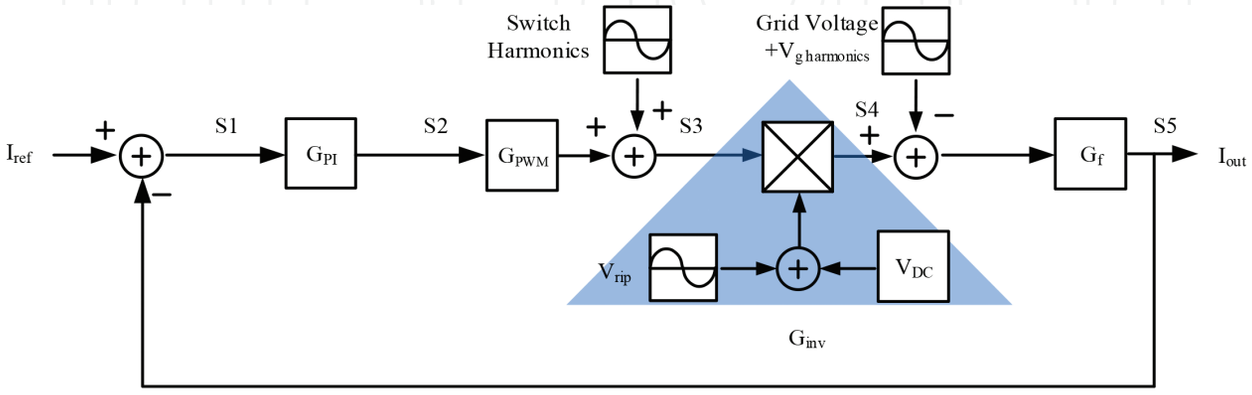

Figure 5. Model of inverter with the DC-link voltage ripple.

$$\begin{aligned} y[n-1] &= [\cos(\omega_o[n-1]) - y[n-1-1]]\,[\cos(2\omega_o[n-1]) + V_{DC}] \\ &= \cos(\omega_o[n-1])[\cos(2\omega_o[n-1]) + V_{DC}] - y[n-2][\cos(2\omega_o[n-1]) + V_{DC}] \end{aligned} \tag{3}$$

Substitute Eq. (3) into Eq. (2)

$$\begin{aligned} y[n] = {} & \cos(\omega_o n)[\cos(2\omega_o n) + V_{DC}] \\ & - \cos(\omega_o[n-1])[\cos(2\omega_o[n-1]) + V_{DC}][\cos(2\omega_o n) + V_{DC}] \\ & + y[n-2][\cos(2\omega_o[n-1]) + V_{DC}][\cos(2\omega_o n) + V_{DC}] \end{aligned} \tag{4}$$

This feedback expression can be expanded into an infinite summation of products given by

$$\begin{aligned} y[n] = {} & \cos(\omega_o n)[\cos(2\omega_o n) + V_{DC}] \\ & - \cos(\omega_o[n-1])[\cos(2\omega_o[n-1]) + V_{DC}][\cos(2\omega_o n) + V_{DC}] \\ & + \cos(\omega_o[n-2])[\cos(2\omega_o[n-2]) + V_{DC}][\cos(2\omega_o[n-1]) + V_{DC}][\cos(2\omega_o n) + V_{DC}] \\ & - \cos(\omega_o[n-3])[\cos(2\omega_o[n-3]) + V_{DC}][\cos(2\omega_o[n-2]) + V_{DC}][\cos(2\omega_o[n-1]) \\ & + V_{DC}][\cos(2\omega_o n) + V_{DC}] \end{aligned} \tag{5}$$

A series of odd harmonics is caused by this amplitude modulation in a feedback loop. In Eq. (5), the first product term is illustrated as an example. According to Euler's formula, this term can be expressed as the sum of sinusoids with angular velocity ω_o and $3\omega_o$, which is the fundamental and third harmonics.

$$y[n] = \cos(\omega_o n)[\cos(2\omega_o n) + V_{DC}] = \cos(\omega_o n)V_{DC} + \frac{1}{2}\cos(3\omega_o n) + \frac{1}{2}\cos(\omega_o n) \tag{6}$$

The closed-form solution is derived based on an idea which is similar to the harmonic balance method for radio frequency (RF) circuit [25]. The harmonic balance method is a frequency domain method for calculating steady states of a nonlinear circuit.

All the signals in the control loop can be expressed in polar forms by taking a Fourier transform. The high-order harmonics will be attenuated by the feedback loop, and only the low-order harmonics will be considered. The low-pass filter (LPF) can be assumed as an ideal filter, which can eliminate all the harmonics above a certain order. A finite number of equations can be

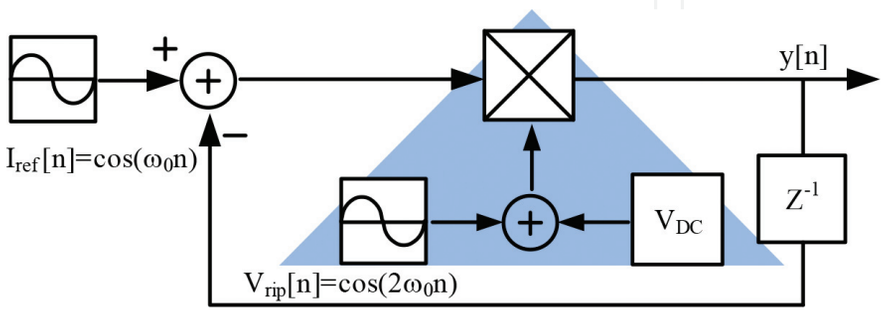

Figure 6. Amplitude modulation in unit delay feedback.

obtained by using this assumption, and a partial linearization for the control loop can be achieved. The amplitude of the feedback signals can be set as variables. After equating like terms in the equation of the output current and in the preset amplitude of feedback signal, a number of equations can be obtained. By solving these equations, the closed-form solution for the amplitude of a certain order of harmonic can be derived. Detailed analysis of the simplified model by using this method in a time domain is given as follows:

The output signal $y(t)$ of the simplified model is the difference between the current reference $I_{ref}(t)$ and the feedback signal $I_{fb}(t)$ multiplied by the DC-link voltage

$$y(t) = \left(I_{ref}(t) - I_{fb}(t)\right)\left(V_{rip}(t) + V_{DC}\right) \tag{7}$$

The signals in **Figure 6** can be expressed in polar form

$$I_{ref}(t) = A\cos(\omega_o t) = ae^{j\omega_o t} + ae^{-j\omega_o t}, a = \frac{1}{2}A \tag{8}$$

$$V_{rip}(t) = B\cos(2\omega_o t) = be^{j2\omega_o t} + be^{-j2\omega_o t}, b = \frac{1}{2}B \tag{9}$$

where A and B are the amplitudes of $I_{ref}(t)$ and $V_{rip}(t)$. In order to simplify the analysis to a level that is suitable for manual calculation, the feedback signal $I_{fb}(t)$ is assumed to include only fundamental and third harmonics

$$I_{fb}(t) = C_1\cos(\omega_o t) + C_3\cos(3\omega_o t) = c_1e^{j\omega_o t} + c_1e^{-j\omega_o t} + c_3e^{j3\omega_o t} + c_3e^{-j3\omega_o t} \tag{10}$$

where C_1 and C_3 are the assumed variables for the amplitude of the fundamental component and third harmonics, and $c_1 = 0.5C_1$, $c_3 = 0.5C_3$. This can be easily extended to any number of harmonics with the help of computer-aided calculations.

Eq. (11) can be obtained by substituting Eqs. (8)–(10) into Eq. (7). Since the$I_{fb}(t)$ is the low-order part of $y(t)$, the harmonic amplitude equation can be found by equating like terms in Eqs. (10) and (11)

$$\begin{aligned} y(t) = {} & [(V_{DC}+b)(a-c_1) - bc_3]e^{j\omega_o t} + [(V_{DC}+b)(a-c_1) - bc_3]e^{-j\omega_o t} \\ & + [b(a-c_1) - V_{DC}c_3]e^{j3\omega_o t} + [b(a-c_1) - V_{DC}c_3]e^{-j3\omega_o t} - bc_3e^{j5\omega_o t} - bc_3e^{-j5\omega_o t} \end{aligned} \tag{11}$$

$$\begin{cases} c_1 = (V_{DC}+b)(a-c_1) - bc_3 \\ c_3 = b(a-c_1) - V_{DC}c_3 \end{cases} \tag{12}$$

All the parameters are fixed values (a, b and V_{DC}) for a specific inverter; therefore, the harmonic amplitude can be obtained by substituting these values. By using the same method, the closed-form solution for the averaged model in **Figure 5** with PI controller can be derived. Two integral sections will be involved into the calculation due to the integrator in the controller and the filter. This calculation for the practical models becomes significantly complicated, and it is impossible to calculate manually. Matlab can be utilized as an effective tool to conduct these calculations.

4. Simulation and experimental results

In this section, the simulation and experiment results are reported. By using Matlab/Simulink, a single-phase PV inverter is simulated. The switching model simulation provides the most detailed results including the switch information and all the potential harmonic distortions. By using the Simulink SimPowerSystems toolbox, the developed model includes both electronic components and control blocks. The schematic diagram is shown in **Figure 7**. It is a time-consuming process. A 0.2-s simulation period takes about 10 min to run on a computer with average performance (Intel Core 2 Duo CPUs and 4 GB of 800 MHz DDR2 RAM).

The two-stage grid-connected PV system prototype is constructed in the laboratory to verify the abovementioned analysis. It includes a boost converter connected with the full-bridge inverter as the second stage. The operating voltage range of the system has been scaled down due to the limitation in the experimental setup. An AC source with 50 V_{rms} is used as the grid voltage. The full-bridge inverter DC-link voltage is 100 V. The capacitor size has been changed with different capacitance to create different voltage ripple across the DC link. The experimental setup with the prototype circuit is shown in **Figure 8**, which is the same as in **Figure 9**, and the main circuit parameters are shown in **Table 1**. A dSPACE controller set has been used to control these two stages.

An averaged model has also been built in Simulink. The parameters listed in **Table 1** are substituted into the derived closed-form solution in order to calculate the harmonics. Different levels of DC-link voltage ripple in simulation and experiment have been created by using different sizes of capacitors. Only the third-order harmonics from the fast Fourier transform (FFT) analysis is considered in calculating the THD, in order to simplify the analysis process. In

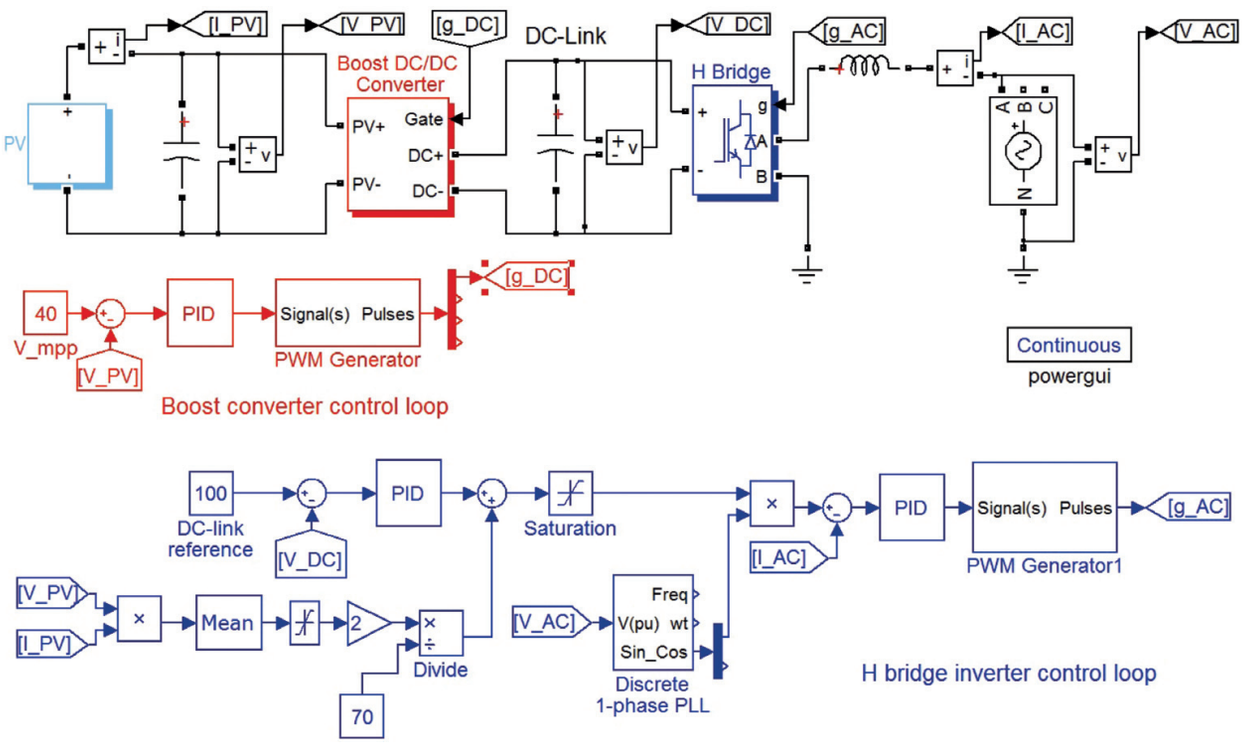

Figure 7. Simulation schematic model.

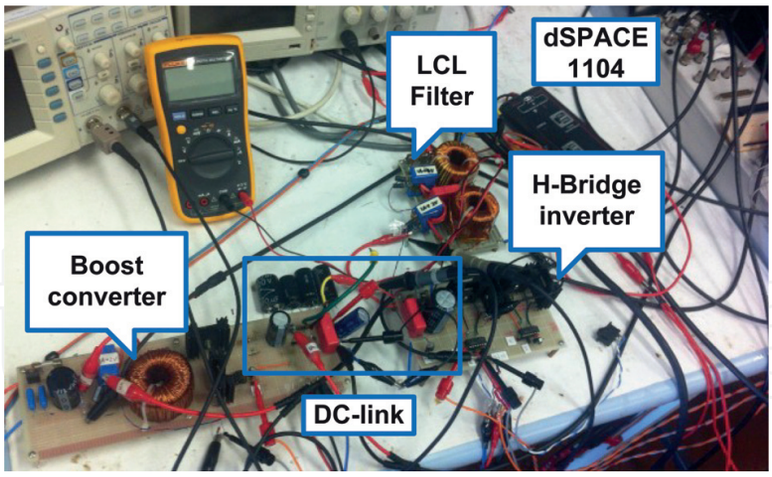

Figure 8. Experimental setup.

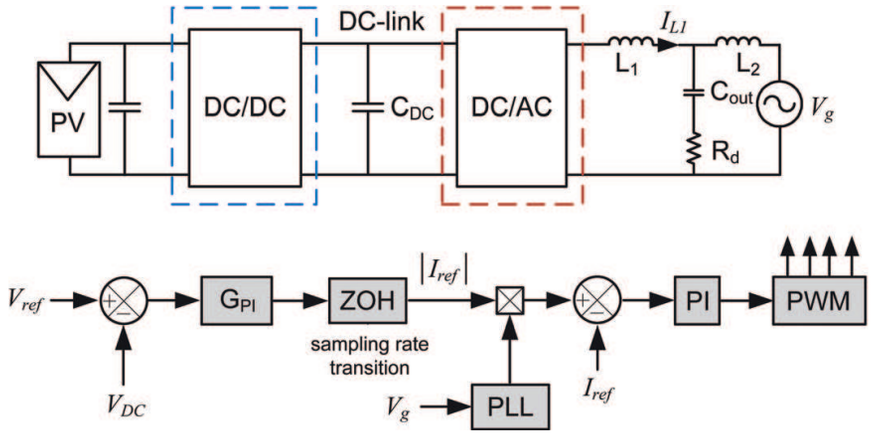

Figure 9. Two-stage PV inverter with feedback control.

Parameter	Label	Value	Unit
Switching frequency	f_{sw}	20	kHz
Rated output frequency	f	50	Hz
Rated output voltage	V_g	70	V
DC-link capacitance	C_{DC}	770	μF
DC-link voltage	V_{DC}	100	V
Inverter-side inductor	L_1	2.56	mH
Grid-side inductor	L_2	1.10	mH
Output capacitor	C_{out}	2.2	μF
Damping resistor	R_d	1	Ω

Table 1. Specification of the PV inverter.

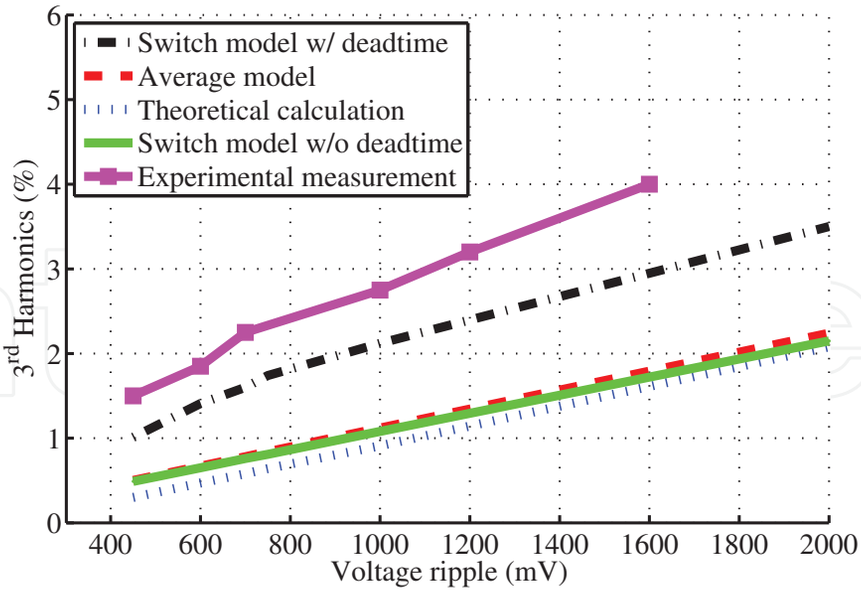

Figure 10. Simulation, calculation, and experimental results.

Figure 10, the switch model, averaged model, and calculation results agree with one another. It proves that the closed-form solution can fully represent the switch model for harmonic analysis. Higher-order harmonics also can be analyzed by using the same method.

The same parameters as the simulation have been used in the experiment, and the results are also plotted in **Figure 10**. The experimental results show the same trend as the analysis suggests that the harmonic distortion increases as the DC-link voltage increases.

5. Conclusion

In this chapter, a general model, which is modified from a conventional control structure diagram, has been introduced to analyze the harmonic generation process caused by single-phase PV inverter. The causes of the harmonics have been identified. A series of odd harmonics in the output current on the DC-link capacitor are generated by the double-line frequency voltage ripple. In this chapter, a nonlinear, time-varying model and its closed-form solution were provided. The relationship between the amplitude of the harmonics and the DC-link voltage ripples has been presented. The proposed solutions are proved by both experimental and simulation results. It is a tool for evaluating the power-quality issues in grid-connected inverter systems. The designers can also use it to consider the tradeoff between the size of the DC-link capacitor and the output harmonics in the output current.

Acknowledgements

This research was supported by the University Research Development Fund (RDF-15-01-40) from the Xi'an Jiaotong-Liverpool University and Jiangsu University S&T programme (17KJB470012).

Author details

Yang Du[1]* and Dylan Dah-Chuan Lu[2]

*Address all correspondence to: yang.du@xjtlu.edu.cn

1 Xi'an Jiaotong-Liverpool University, Suzhou, China

2 University of Technology Sydney, Australia

References

[1] Du Y, Lu DDC, Cornforth D, James G. A study on the harmonic issues at CSIRO microgrid. IEEE 9th International Conference on Power Electronics and Drive Systems (PEDS). 2011:203-207

[2] Du Y, Lu DD-C. Battery-integrated boost converter utilizing distributed MPPT configuration for photovoltaic systems. Solar Energy. 2011;**85**(9):1992-2002

[3] Bennett T, Zilouchian A, Messenger R. Photovoltaic model and converter topology considerations for MPPT purposes. Solar Energy. 2012;**86**(7):2029-2040

[4] Lu DDC, Nguyen QN. A photovoltaic panel emulator using a buck-boost DC/DC converter and a low cost micro-controller. Solar Energy. 2012;**86**(5):1477-1484

[5] Papaioannou IT, Alexiadis MC, Demoulias CS, Labridis DP, Dokopoulos PS. Modeling and measurement of small photovoltaic systems and penetration scenarios. Power Tech conference, Bucharest. 2009:1-7

[6] Jain SK, Singh SN. Harmonics estimation in emerging power system: Key issues and challenges. Electric Power Systems Research. 2011;**81**(9):1754-1766

[7] Chicco G, Schlabbach J, Spertino F. Experimental assessment of the waveform distortion in grid-connected photovoltaic installations. Solar Energy. 2009;**83**(7):1026-1039

[8] Infield DG, Onions P, Simmons AD, Smith GA. Power quality from multiple grid-connected single-phase inverters. IEEE Transactions on Power Delivery. 2004;**19**(4):1983-1989

[9] Wu TF, Sun KH, Kuo CL, Yu GR. Current distortion improvement and dc-link voltage regulation for bi-directional inverter in dc-microgrid applications. Applied Power Electronics Conference and Exposition (APEC). 2011:1582-1587

[10] Twining E, Holmes DG. Grid current regulation of a three-phase voltage source inverter with an LCL input filter. IEEE Transactions on Power Electronics. 2003;**18**(3):888-895

[11] Shimizu T, Wada K, Nakamura N. Flyback-type single-phase utility interactive inverter with power pulsation decoupling on the DC input for an AC photovoltaic module system. IEEE Transactions on Power Electronics. 2006;**21**(5):1264-1272

[12] Du Y, Lu DD-C, James G, Cornforth DJ. Modeling and analysis of current harmonic distortion from grid connected PV inverters under different operating conditions. Solar Energy. 2013;**94**(0):182-194

[13] Du Y, Lu D, Chu G, Xiao W. Closed-Form Solution of Time-Varying Model and its Applications for Output Current Harmonics in two-Stage PV Inverter. IEEE Transaction on Sustainable Energy; 2015

[14] Lahyani A, Venet P, Grellet G, Viverge PJ. Failure prediction of electrolytic capacitors during operation of a switch mode power supply. IEEE Transactions on Power Electronics. 1998;**13**(6):1199-1207

[15] Hu H, Harb S, Kutkut N, Batarseh I, Shen ZJ. Power decoupling techniques for micro-inverters in PV systems-a review. IEEE Energy Conversion Congress and Exposition (ECCE). 2010:3235-3240

[16] Jiang Y, Ekstrom A. General analysis of harmonic transfer through converters. IEEE Transactions on Power Electronics. 1997;**12**(2):287-293

[17] Wang F, Duarte JL, Hendrix MAM, Ribeiro PF. Modeling and analysis of grid harmonic distortion impact of aggregated DG inverters. IEEE Transactions on Power Electronics. 2011;**26**(3):786-797

[18] Enjeti PN, Shireen W. A new technique to reject DC-link voltage ripple for inverters operating on programmed PWM waveforms. IEEE Transactions on Power Electronics. 1992;**7**(1):171-180

[19] Brekken T, Bhiwapurkar N, Rathi M, Mohan N, Henze C, Moumneh LR. Utility-connected power converter for maximizing power transfer from a photovoltaic source while drawing ripple-free current. In: IEEE 33rd Annual Power Electronics Specialists Conference (PESC). 2002. pp. 1518–1522 vol.3

[20] Zhao W, Lu DDC, Agelidis VG. Current control of grid-connected boost inverter with zero steady-state error. IEEE Transactions on Power Electronics. 2011;**26**(10):2825-2834

[21] Armstrong M, Atkinson DJ, Johnson CM, Abeyasekera TD. Low order harmonic cancellation in a grid connected multiple inverter system via current control parameter randomization. IEEE Transactions on Power Electronics. 2005;**20**(4):885-892

[22] Maknouninejad A, Kutkut N, Batarseh I, Zhihua Q, Shoubaki E. Detailed analysis of inverter linear control loops design. Applied Power Electronics Conference and Exposition (APEC). 2011:1188-1193

[23] McGrath BP, Holmes DG. A general analytical method for calculating inverter dc-link current harmonics. IEEE Transactions on Industry Applications. 2009;**45**(5):1851-1859

[24] Kleimola J, Lazzarini V, Valimaki V, Timoney J. Feedback amplitude modulation synthesis. EURASIP Journal on Advances in Signal Processing. 2011;**2011**(1):434378

[25] Maas SA. Nonlinear Microwave and RF Circuits: Artech House Publishers; 2003